Biophysical Chemistry 184 (2013) 68–78

Contents lists available at ScienceDirect

Biophysical Chemistry

journal homepage: http://www.elsevier.com/locate/biophyschem

Detailed kinetic analysis of the interaction between the FOXO4–DNA-binding domain and DNA

Petr Vacha [a], Iva Zuskova [a,b], Ladislav Bumba [c], Petr Herman [d], Jaroslav Vecer [d], Veronika Obsilova [b], Tomas Obsil [a,b,*]

[a] Department of Physical and Macromolecular Chemistry, Faculty of Science, Charles University in Prague, 12843 Prague, Czech Republic
[b] Institute of Physiology, Academy of Sciences of the Czech Republic, 14220 Prague, Czech Republic
[c] Institute of Microbiology, Academy of Sciences of the Czech Republic, 14220 Prague, Czech Republic
[d] Faculty of Mathematics and Physics, Institute of Physics, Charles University in Prague, 12116 Prague, Czech Republic

HIGHLIGHTS

- Interaction between FOXO4 and DNA is described using a conformational change model.
- FOXO4–DBD undergoes a conformational change upon binding to the DNA.
- Segmental dynamics of FOXO4–DBD is reduced upon binding to the DNA.
- Non-specific contacts are important for binding affinity and specificity of FOXO4.

GRAPHICAL ABSTRACT

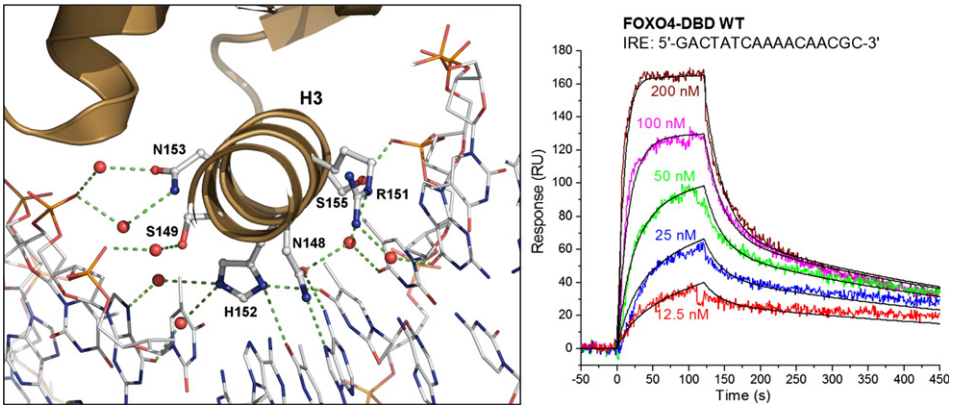

ARTICLE INFO

Article history:
Received 26 July 2013
Received in revised form 5 September 2013
Accepted 5 September 2013
Available online 15 September 2013

Keywords:
FOXO4 forkhead transcription factor
DNA-binding domain
Binding kinetics
Surface plasmon resonance
Time-resolved fluorescence
Segmental dynamics

ABSTRACT

The FOXO forkhead transcription factors are potent transcriptional activators involved in a wide range of key biological processes. In this work, the real-time kinetics of the interaction between the FOXO4–DNA binding domain (FOXO4–DBD) and the DNA was studied by using surface plasmon resonance (SPR). SPR analysis revealed that the interaction between FOXO4–DBD and the double stranded DNA containing either the insulin-responsive or the Daf-16 family member-binding element is preferably described by using a conformational change model which suggests a structural change of FOXO4–DBD upon binding to the DNA. This was further confirmed by using the time-resolved tryptophan fluorescence anisotropy decay measurements which revealed profound reduction of segmental dynamics of FOXO4–DBD upon the complex formation. Alanine scanning of amino acid residues engaged in polar contacts with the DNA showed that certain non-specific contacts with the DNA backbone are very important for both the binding affinity and the binding specificity of FOXO4–DBD.

1. Introduction

The FOXO transcription factors (FOXO1, FOXO3, FOXO4 and FOXO6) are potent transcriptional activators involved in a wide range of processes including energy metabolism control, DNA damage repair, cellular

* Corresponding author at: Department of Physical and Macromolecular Chemistry, Faculty of Science, Charles University in Prague, 12843 Prague, Czech Republic. Tel.: +420 221951303; fax: +420 224919752.
E-mail address: obsil@natur.cuni.cz (T. Obsil).

0301-4622/$ – see front matter © 2013 Elsevier B.V. All rights reserved.
http://dx.doi.org/10.1016/j.bpc.2013.09.002

proliferation, cell survival and stress resistance [1]. The FOXO proteins are members of the "O" subclass of the forkhead protein family (FOX) that comprises more than 100 proteins that are further classified into 17 subclasses (designated A–Q). All FOX proteins share a highly conserved DNA-binding domain (DBD), also known as the forkhead box or winged-helix domain, that possesses a compact α/β fold and recognizes sequences containing the core motif 5′-(A/C)AA(C/T)A-3′ through a combination of direct and water-mediated side chain-base contacts [2,3]. The high conservation of forkhead DNA-binding domains as well as their binding motifs together with the large diversity of the biological processes the FOX proteins are involved in suggest the existence of a high degree of binding specificity [4]. Fine variations in binding affinity for different DNA response elements might be an important factor involved in the regulation of target gene expression by FOX proteins. Such mode of regulation has been shown, for example, for FoxA protein in the control of organogenesis [5]. However, factors underlying intrinsic variations in binding affinity of forkhead domains for different but very similar binding motifs are still not fully understood.

The most important part of the DNA-binding interface of forkhead domain is the helix H3, which binds into the major groove roughly perpendicular to the DNA axis and provides the principal contact surface with the core motif [3]. Residues involved in these interactions are conserved among all forkhead proteins and make a combination of direct and water-mediated side chain–base contacts. Additional contacts with the DNA are made by residues from other parts of the domain including N-terminal segment, helices H1 and H2, and both flexible loops called wings W1 and W2. In addition, the forkhead domain binding narrows the major groove in which the helix H3 is located and induces a significant bend of the DNA. Members of FOXO subclass recognize two consensus motifs: 5′-(C/A)(A/C)AAA(C/T)AA-3′, known as the insulin-responsive sequence (IRE) [6,7], and 5′-GTAAA(T/C)AA-3′, known as the Daf-16 family member-binding element (DBE) [8,9]. Although both these sequences are closely related and include the core sequence, FOXO proteins bind the DBE sequence with higher affinity. Structural studies of FOXO–DBD–DNA complexes revealed expected mode of DNA recognition with residues from the helix H3 (N148 and H152 in FOXO4) making all direct base-specific contacts with the core sequence [10–12]. Other parts of FOXO–DBD DNA-binding interface include the N-terminal segment and both loops W1 and W2 that are involved in non-specific contacts with the phosphate groups of DNA backbone (Fig. 1). Solution structures of FOXO–DBD showed that the N-terminal segment, the loop W1 and especially the loop W2 are in the absence of DNA highly flexible [13,14]. The loop W2 is very important for the high-affinity binding of FOXO–DBD to the DNA, although being highly flexible and mostly disordered also in the presence of the DNA [11,15]. In addition, the loop between helices H2 and H3 adopts in apo-structures helical conformation while in the DNA-bound

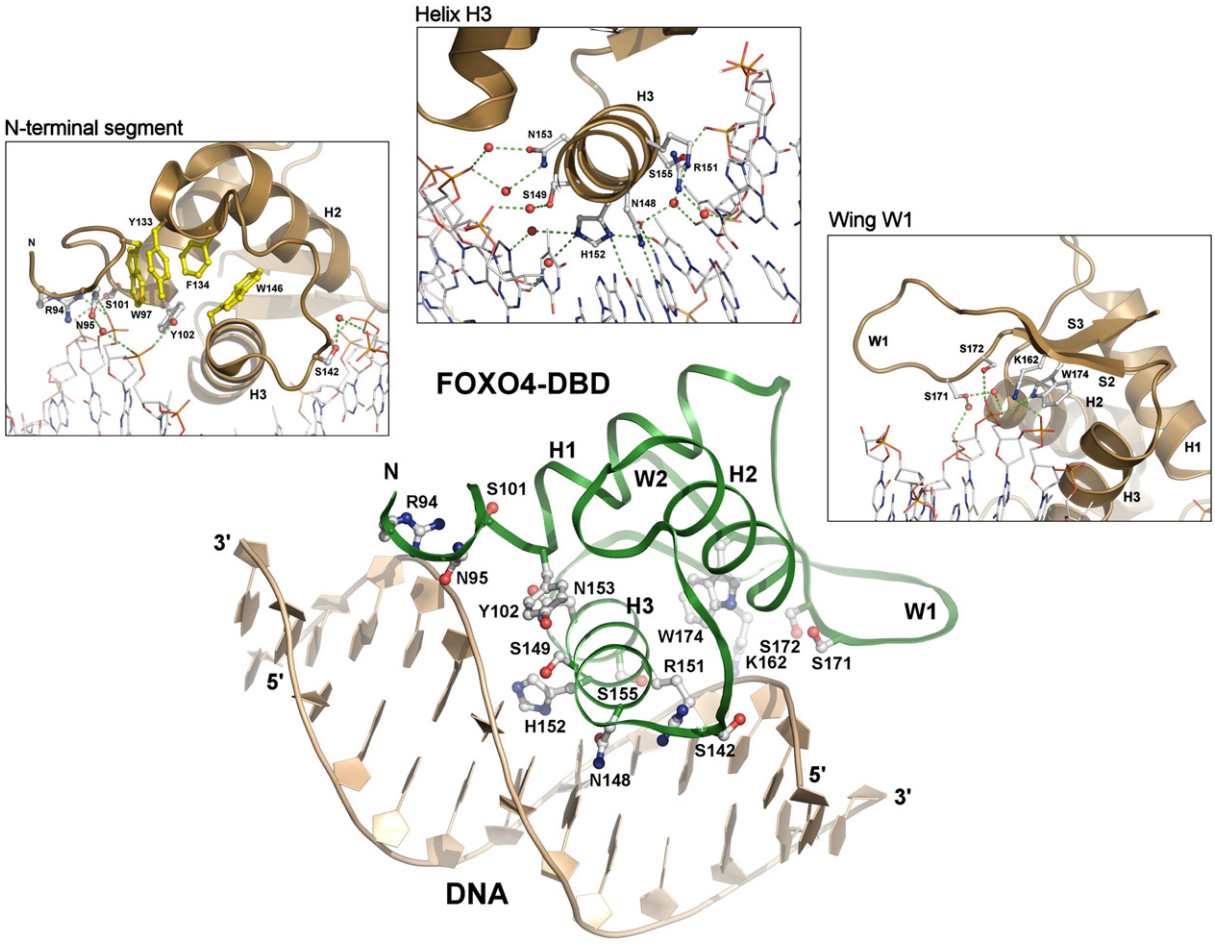

Fig. 1. The crystal structure of the FOXO4–DBD–DNA complex [12]. Both the forkhead domain (green) and dsDNA (brown) are shown in ribbon representation. Secondary-structure elements are labeled according to the nomenclature typical for the winged–helix motif. All residues of FOXO4–DBD that are involved in polar contacts with the DNA are shown as sticks and spheres. Insets: Binding interface of the FOXO4–DBD–DNA complex. The backbone of FOXO4–DBD, the interacting amino acid side chains of FOXO4–DBD and dsDNA are shown in cartoon (brown), sticks and lines representation, respectively. A cluster of hydrophobic residues surrounding Y102 is shown in yellow. Water molecules are represented as red spheres. Polar contacts between FOXO4–DBD and DNA are represented by dashed green lines.

complexes is unstructured. All these indicate that FOXO–DBD undergoes a structural transition during the binding to the DNA.

The FOXO–DBD–DNA interaction studies were focused so far mostly on base-specific contacts and sites of post-translational modifications within the DNA-binding interface [10,11,15–17]. However, it has been shown that non-DNA contact regions and non-specific contacts might affect the binding specificity and affinity of forkhead proteins through the repositioning of regions containing recognition elements (helix H3) and/or through the modulation of the dissociation rate of the protein–DNA complexes [18–21]. In order to better understand factors underlying FOXO's variations in affinity for different but closely related DNA sequences and especially the possible role of non-specific contacts, we performed alanine scanning mutagenesis of FOXO4–DBD amino acid residues engaged in polar contacts with the DNA followed by surface plasmon resonance (SPR) analysis. The real-time kinetics data revealed that the interaction between FOXO4–DBD and the double stranded DNA containing either IRE or DBE motif is preferably described by using a conformational change model which suggests a structural change of FOXO4–DBD upon binding to the DNA. Our SPR data show that all parts of the DNA-binding surface of FOXO4–DBD are important for the overall stability of the FOXO4–DBD–DNA complex and that certain non-specific contacts with the DNA backbone are very important for both the binding affinity and the binding specificity of FOXO4–DBD. The predominant mechanism that contributes to the decreased binding affinity upon the disruption of these contacts is the faster dissociation rate of the encounter complex compared to the wild-type.

2. Materials and methods

2.1. Expression and purification of FOXO4–DBD

The human FOXO4–DBD (sequence 82–207) and all its mutant versions were expressed as described previously [12,15]. Briefly, FOXO4–DBD was expressed as N-terminal 6 × His-tag fusion proteins by IPTG induction for 20 h at 20 °C and purified from *Escherichia coli* BL21 (DE3) cells using Chelating Sepharose Fast Flow (GE Healthcare Life Sciences) according to the standard protocol. Eluted FOXO4–DBD was dialyzed against the buffer containing 50 mM sodium citrate (pH 6.3), 1 mM EDTA, 2 mM DTT and purified using cation-exchange chromatography on SP-Sepharose column (GE Healthcare Life Sciences). The final step, size-exclusion chromatography on Superdex 200 column (GE Healthcare Life Sciences), was performed in buffer containing 20 mM Tris–HCl (pH 7.5), 100 mM NaCl, 1 mM EDTA, 2 mM DTT, and 10% (w/v) glycerol. All mutants were generated by using the QuikChange kit (Stratagene) and mutations were confirmed by sequencing.

2.2. Surface plasmon resonance (SPR)

All SPR measurements were performed at 25 °C using a double-stranded DNA-coated LCP sensor chip mounted on a ProteOn XPR36 Protein Interaction Array System (Bio-Rad, Hercules, CA, USA). The double stranded DNA (dsDNA) was prepared by mixing of two complementary oligonucleotides in a molar ratio of 1:1 at 70 °C for 10 min and slowly (~20 min) cooled down to room temperature. The oligonucleotides were purchased from VBC Biotech (Vienna, Austria), and for dsDNA carrying IRE motif (underlined), oligonucleotides 5′-GACTATCAAAACAACGC-3′ modified at 5′ end by biotin and 5′-GCGTTGTTTTGATAGTC-3′; for dsDNA carrying DBE sequence (underlined), oligonucleotides 5′-GACTATGTAAACAACGC-3′ modified at 5′ end by biotin and 5′-GCGTTGTTTACATAGTC-3′; and for a control (random) dsDNA, oligonucleotides 5′-AACGTATGCTCTAGCCA-3′ modified at 5′ end by biotin and 5′-TGGCTAGAGCATACGTT-3′ were used, respectively. Biotinylated dsDNA was diluted to a final concentration of 100 nM in PBS buffer containing 0.05% Tween 20 and captured to a neutravidin-functionalized LCP chip at a flow rate of 30 μl/min for 2 min. Loosely attached material was removed from the chip surface by two injections of 60 μl of 2 M NaCl. All SPR measurements were carried out in running buffer containing 20 mM Tris–HCl (pH 7.5), 150 mM NaCl, 0.1 mM EDTA, 2 mM DTT and 0.005% Tween-20 at the flow rate ranging from 25 to 75 μl/min for both association and dissociation phase of sensograms. The proteins were serially diluted in running buffer to indicated concentrations (200, 100, 50, 25 and 12.5 nM), and injected in parallel ("one-shot kinetics") over the immobilized dsDNA surface. Surfaces were typically regenerated with 100 μl of 2 M NaCl. The sensograms were corrected for sensor background by interspot referencing (the sites within the 6 × 6 array which are not exposed to ligand immobilization but are exposed to analyte flow), and double referenced by subtraction of analyte (channels 1–5) using a "blank" injection (channel 6).

The data were analyzed globally by fitting both the association and the dissociation phases simultaneously for five different FOXO4–DBD concentrations using both a 1:1 Langmuir-type binding model and the conformational change model to determine the kinetics association and dissociation rate constants. The Langmuir-type model assumes the interaction between protein (A) and DNA (B) resulting in a direct formation of the final complex (AB):

$$A + B \underset{k_d}{\overset{k_a}{\rightleftarrows}} AB, \tag{1}$$

where k_a and k_d are the association and the dissociation rate constants, respectively. The conformational change model assumes the two-step association process:

$$A + B \underset{k_{d1}}{\overset{k_{a1}}{\rightleftarrows}} [AB]* \underset{k_{d2}}{\overset{k_{a2}}{\rightleftarrows}} AB, \tag{2}$$

where [AB]* and AB represent encounter complex (transition state) and final docked state, respectively [22–24]. Parameters k_{a1} and k_{d1} are the association and the dissociation rate constants for the first step (encounter complex formation), while k_{a2} and k_{d2} are forward and reverse rate constants for the second step (conformational change). An apparent equilibrium dissociation constant, K_D, for the 1:1 Langmuir-type binding was determined as

$$K_D = k_d/k_a, \tag{3}$$

and for the conformational change binding model as

$$K_D = 1/[(k_{a1}/k_{d1})\times(1 + k_{a2}/k_{d2})]. \tag{4}$$

Detailed description of both binding models including the rate equations and the description of the fitting procedure is shown in the supplementary material.

2.3. Time-resolved fluorescence measurements

Fluorescence intensity and anisotropy decays were measured on a time-correlated single photon counting apparatus, as described previously [25]. Tryptophan emission was excited at 298 nm by the third harmonic of the Ti:Sapphire laser emitting at 894 nm. Tryptophan fluorescence was collected at 355 nm using a monochromator equipped with a stack of UG1and BG40 glass filters (Thorlabs) placed in front of its input slit. Typically, the decays were accumulated in 1024 channels with time resolution of 50 ps per channel until 10^7 counts per decay were reached. Samples were placed in a thermostatic holder, and all experiments were performed at 23 °C in a buffer containing 20 mM Tris–HCl (pH 7.5), 150 mM NaCl, 0.1 mM EDTA, and 2 mM DTT. The FOXO4–DBD concentration was 5 μM, and the dsDNA concentration was 15 μM. The following oligonucleotides containing consensus IRE motif (underlined) were used to prepare samples of dsDNA: 5′-GACTATCAAAACAACGC-3′ and 5′-GCGTTGTTTTGATAGTC-3′. The fluorescence decays were acquired

under magic-angle conditions in which the measured intensity decay, $I(t)$, is independent of the rotational diffusion of the chromophore and provides true lifetime information. Fluorescence was assumed to decay multiexponentially according to the formula

$$I(t) = \sum_i \alpha_i \times \exp(-t/\tau_i), \quad (5)$$

where τ_i and α_i are the fluorescence lifetimes and the corresponding amplitudes, respectively. A maximum entropy method was used to analyze $I(t)$ [26]. The program yields amplitudes, α_i, that represent the lifetime distribution. We chose 100 lifetimes equidistantly spaced in the logarithmic scale, covering the range from 20 ps to 20 ns. The mean lifetime was calculated as follows:

$$\tau_{mean} = \sum_i f_i \tau_i = \sum_i \left(\alpha_i \tau_i^2\right) / \sum_i (\alpha_i \tau_i), \quad (6)$$

where f_i is the fractional intensity of the ith lifetime component. The polarized components $I_{\|}(t)$ and $I_{\perp}(t)$ required for the construction of the fluorescence anisotropy $r(t)$ were accumulated quasi-simultaneously with a switching frequency of 30 s. The polarized decays were measured with the emission polarizer set in the fixed vertical position, and excitation polarization plane was rotated 0° and 90°, respectively. This approach minimized the need to correct transmittances of the detection channel for different polarizations, because the G-factor was close to one. The value of the G-factor was determined in an independent experiment. The fluorescence anisotropy decays $r(t)$ were obtained by simultaneous reconvolution analysis of both parallel $I_{\|}(t)$ and perpendicular $I_{\perp}(t)$ decay components. Data were analyzed by a model-independent maximum entropy method that does not set prior limits on the shape of the distributions [26]. The anisotropies $r(t)$ were analyzed for a series of exponentials:

$$r(t) = \sum_i \beta_i \times \exp(-t/\varphi_i), \quad (7)$$

where the amplitudes β_i represent the distribution of the correlation times ϕ_i and are related to the initial anisotropy r_0 by the formula

$$\sum_i \beta_i = r_0. \quad (8)$$

We used 100 correlation times ϕ_i equidistantly spaced in the logarithmic scale ranging from 50 ps to 200 ns.

2.4. Circular dichroism spectroscopy

Circular dichroism (CD) measurements were carried out as described previously [27]. Briefly, the CD spectra were measured in a quartz cuvette with an optical path length of 1 mm (Starna, USA) using a J-810 spectrometer (Jasco, Japan). The conditions of the measurements were as follows: a spectral region of 200–320 nm, a scanning speed of 10 nm/min, a response time of 8 s, a resolution of 1 nm, a bandwidth of 1 nm and a sensitivity of 100 mdeg. The final spectrum was obtained as an average of 5 accumulations. The spectra were corrected for a baseline by subtracting the spectra of the corresponding polypeptide-free solution. The spectra were recorded at room temperature (23 °C) in a buffer containing 20 mM Tris–HCl (pH 7.5), 150 mM NaCl, 0.1 mM EDTA, 2 mM 2-mercaptoethanol, and 10% (w/v) glycerol. The FOXO4–DBD concentration was 6 μM.

3. Results

3.1. Site-directed mutagenesis of FOXO4–DBD

The importance of various residues in FOXO–DBD for its binding to the target DNA has already been investigated by several groups, but only for residues that are either involved in base-specific contacts or serve as sites of post-translational modifications [10,11,15–17]. However, neither detailed kinetic analysis nor the evaluation of the role of non-specific contacts (contacts to the phosphate groups of the DNA) for the binding affinity and specificity of FOXO–DBD were published so far. In order to evaluate the importance of these contacts on the stability of FOXO–DBD–DNA complexes, the amino acids involved in both specific and non-specific polar contacts between FOXO4–DBD and DNA [12] were substituted to alanine residue (with the exception of Y102 which was replaced by Phe), and the real-time binding kinetics of individual FOXO4–DBD mutants were analyzed by using surface plasmon resonance (SPR). The list of the FOXO4–DBD mutants and the type of interaction between the side-chain of the mutated residue and DNA are shown in Table 1. The expression yield as well as the solubility of all prepared mutants were unchanged compared to FOXO4–DBD WT. Structural integrity of prepared proteins was verified by using circular dichroism (CD) measurements. Supplemental Fig. S1 shows the far-UV CD spectra of FOXO4–DBD WT and mutants that exhibit the most profound change in DNA-binding affinity. As can be noticed the CD spectra of these mutants showed no significant differences compared to WT.

3.2. Kinetics of interaction between FOXO4–DBD and DNA

Interactions of FOXO4–DBD with DNA were studied by immobilization of biotinylated double-stranded DNA (dsDNA) containing a random sequence, IRE or DBE motif, respectively, on the neutravidin-coupled LCP sensor chip. To minimize non-specific binding and mass transfer effect, three coupling concentrations of dsDNA leading to refractive index changes of 30, 80, and 150 RU were tested. Initial experiments at each of these dsDNA-coating concentrations were conducted with FOXO4–DBD at concentrations ranging from 10 to 200 nM. Initial estimates of k_{off} values showed concentration dependence at coupling levels of 80 and 150 RU which indicating mass transfer effects.

Table 1
FOXO4–DBD mutants used in the SPR analysis.

FOXO4–DBD mutant	Secondary structure element[a]	Type of the polar contact(s)[b]
R94A	NT	SC–DNA(P)/ES
N95A	NT	SC–DNA(P), SC–W–DNA(P)
S101A	H1	SC–W–DNA(P)
Y102F	H1	SC–DNA(P)
S142A	H2–H3	SC–DNA(P), SC–W–DNA(P)
N148A	H3	SC–DNA(B), SC–W–DNA(B)
S149A	H3	SC–W–DNA(P)
R151A	H3	SC–W–DNA(B)
H152A	H3	SC–DNA(B), SC–W–DNA(B)
N153A	H3	SC–W–DNA(P)
S155A	H3	SC–DNA(P)
K162A	S2	SC–DNA(P)/ES
S171A	W1	SC–W–DNA(P)
S172A	W1	SC–DNA(P)
ΔC (82–183)	W2 (missing)	1× SC–DNA(P)/ES, 1× ES, 2× SC–DNA(P)[c]

[a] NT, N-terminal loop; H1, α-helix H1; H2–H3, loop between α-helices H2 and H3; H3, α-helix H3, S2, β-strand S2; W1, wing W1; W2, wing W2.
[b] SC–DNA(P), a hydrogen bond between the side chain and the phosphate group; SC–W–DNA(P), a water mediated interaction between the side chain and the phosphate group; SC–DNA(B), a hydrogen bond between the side chain and the base; SC–W–DNA(B), a water mediated base-specific interaction; ES, electrostatic interaction.
[c] Based on crystal structure of the FOXO3–DBD–DNA complex [10].

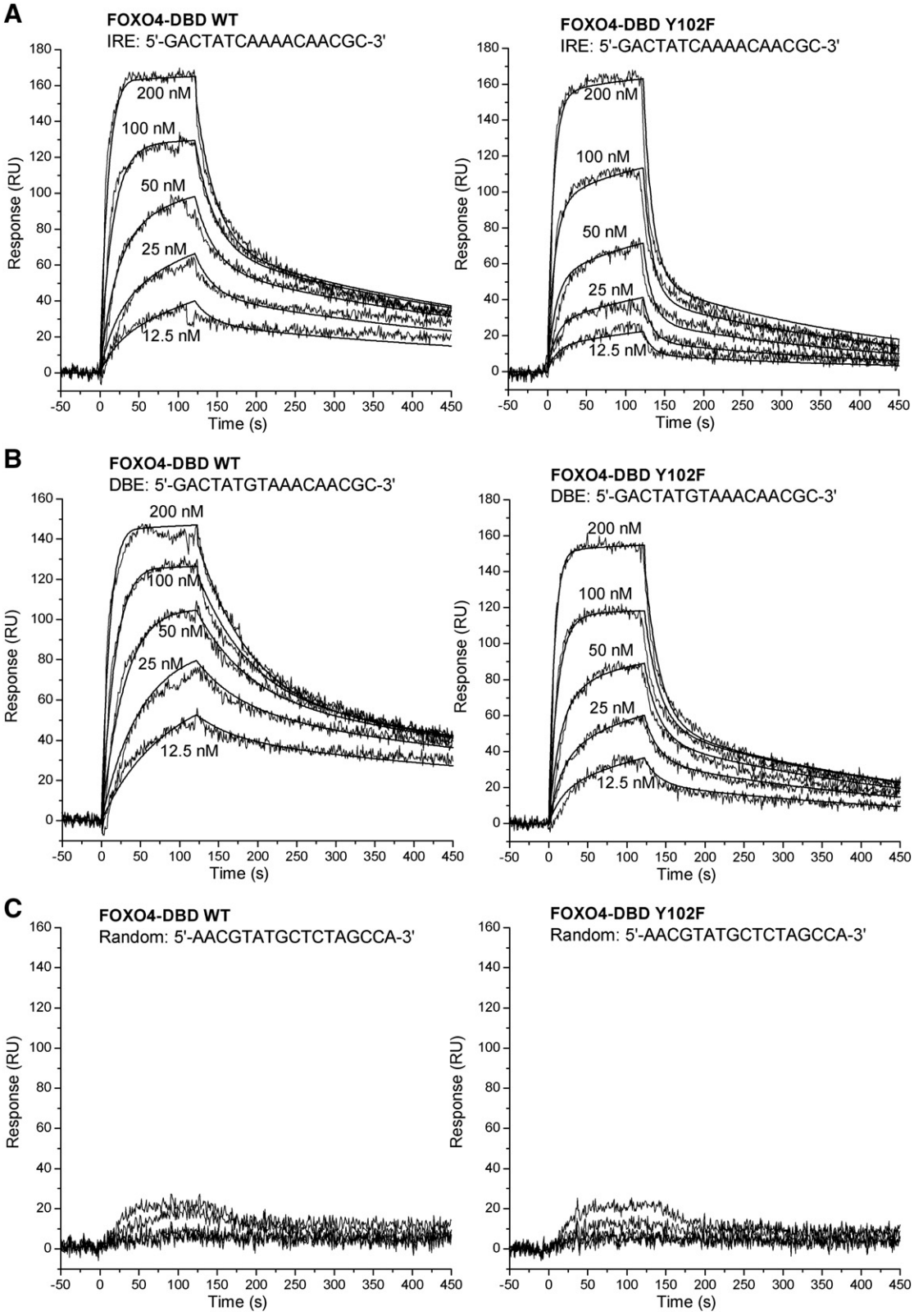

Fig. 2. SPR kinetic binding analysis of the interaction between DNA and FOXO4–DNA–binding domain (DBD). One-shot kinetics data of the wild-type FOXO4–DBD (left column) and the FOXO4–DBD–Y102F mutant (right column) interacting with dsDNA containing the insulin-responsive (A), the Daf-16 family member-binding element (B), and dsDNA containing a random DNA sequence (C). The proteins at indicated concentrations were injected in parallel over the sensor chip coated with dsDNA and the flow rate was maintained at 50 μl/min for both association and dissociation phases of the sensograms. The kinetic data were globally fitted by using a conformational change model (see Materials and methods). The fitted curves are superimposed as thin black line on top of the sensograms.

However, coupling level of 30 RU resulted in clear responses and concentration independence of k_{off} at flow rates ranging from 25 to 75 μl/ml (data not shown). Consequently, coupling level of 30 RU and flow rate of 50 μl/ml were used for the remaining experiments.

Real time interaction of FOXO4–DBD with the IRE and DBE sequence revealed a typical association and dissociation phases of the sensogram (Fig. 2). Binding was specific, since negligible binding of FOXO4–DBD was detected to the chip coated with the random dsDNA sequence (Fig. 2C). Kinetic parameters of the FOXO4–DBD–DNA interactions were calculated from global fitting of concentration-dependent binding curves. The data were fitted to both a simple 1:1 Langmuir-type binding model (Eq. (1)) and a conformational change model (Eq. (2)). We found that the interaction between FOXO4–DBD and both used dsDNAs is significantly better described (in terms of reduced χ^2 and residual statistics) by the conformational change model compared to the 1:1 Langmuir-type model. The fits of the conformational change binding model to the SPR data of FOXO4–DBD WT and FOXO4–DBD Y102F mutant binding to IRE and DBE are shown as an example in Fig. 2A and B. The fits of the 1:1 Langmuir-type binding model to the same SPR data as well as the residual plots of these fits are shown in Fig. S2. To prove the conformational change model by SPR, variation in the injection times at high concentration of FOXO4–DBD (300 nM) were investigated for both IRE and DBE sequences. Changing the injection time of the analyte revealed that the dissociation rate was progressively decreased after longer contact time, indicating that the stability of the initial FOXO4–DBD–DNA complexes increases over time (Fig. 3 and Fig. S3).

3.3. Conformational change of FOXO4–DBD upon its binding to the DNA

To further validate the conformational change of FOXO4–DBD upon binding to the DNA, time-resolved tryptophan fluorescence anisotropy decay measurements were used to compare the segmental dynamics (flexibility) of FOXO4–DBD WT in its apo- and DNA-bound states. The FOXO4–DBD contains five tryptophan residues (W97, W126, W146, W173 and W174) that sample various regions of DBD including N-terminal segment, helices H2 and H3, and β-strand S3 (Fig. S4). Since we were unable to prepare mutants containing single Trp residue (simultaneous mutagenesis of four other Trp residues to Phe renders FOXO4–DBD insoluble, presumably due to misfolding) we decided to perform this experiment with FOXO4–DBD WT containing all five tryptophan residues. The time-resolved fluorescence intensity and anisotropy decays were analyzed using a singular-value decomposition maximum entropy method as previously described [26]. The results of these experiments are presented in Table 2 and Figs. 4 and 5. The analysis of the fluorescence anisotropy decays revealed three and two classes of correlation times in the absence and the presence of the DNA, respectively (Table 2 and Fig. 5). Short correlation times located around 0.9–1.3 ns and 2.7 ns reflected the fast local motions of Trp residues. The long correlation time, ϕ_3, likely reflected the rotational diffusion of the whole protein molecule or the protein–DNA complex. The change in the segmental mobility of FOXO–DBD was assessed from the change in the sum of amplitudes of fast anisotropy decay components β_{short} ($\beta_{short} = \beta_1 + \beta_2$). As can be noticed, the binding of FOXO4–DBD to the DNA significantly decreased β_{short} (β_{short}(FOXO4–DBD) = 0.135; β_{short}(FOXO4–DBD–DNA) = 0.059). In addition, the second component of the fluorescence anisotropy decay represented by the correlation time ϕ_2 was absent in the presence of the DNA. These changes can be interpreted as a significant reduction of segmental motions (flexibility) of the whole FOXO4–DBD molecule upon its binding to the DNA, since high mobility of any of the 5 Trps distributed around the whole molecule would lead to a fast fluorescence depolarization and increase of β_{short}. The reduction of flexibility is also well demonstrated in the raw anisotropy decays by the lower decrease of the fluorescence anisotropy at short times after the excitation in the presence of the DNA (Fig. 4). Thus, results of time-resolved fluorescence anisotropy decay measurements strongly suggested that the FOXO4–DBD binding to the DNA is accompanied by structural changes in DBD corroborating the conformational change binding model for FOXO4–DBD–DNA interaction.

In addition, the conformational change model is also fully consistent with the available structural data on FOXO–DBD proteins. The comparison of apo- and DNA-bound structures of FOXO–DBD revealed significant

Table 2
Summary of time-resolved tryptophan fluorescence measurements of FOXO4–DBD.

	τ_{mean}[ac] (ns)	β_1[bd]	ϕ_1[be]	β_2[bd]	ϕ_2[be]	β_3[bd]	ϕ_3[be]
FOXO4–DBD	4.19	0.041	1.3	0.094	2.7	0.076	12
FOXO4–DBD + DNA	3.85	0.059	0.9	–	–	0.147	19

[a] The mean fluorescence lifetime (τ_{mean}) was calculated using Eq. (6).
[b] The fluorescence anisotropies $r(t)$ were analyzed for series of exponentials (Eq. (7)), where the amplitudes β_i represent the distribution of the correlation times ϕ_i.
[c] SD < 0.05 ns.
[d] SD < 0.01.
[e] SD < 20%.

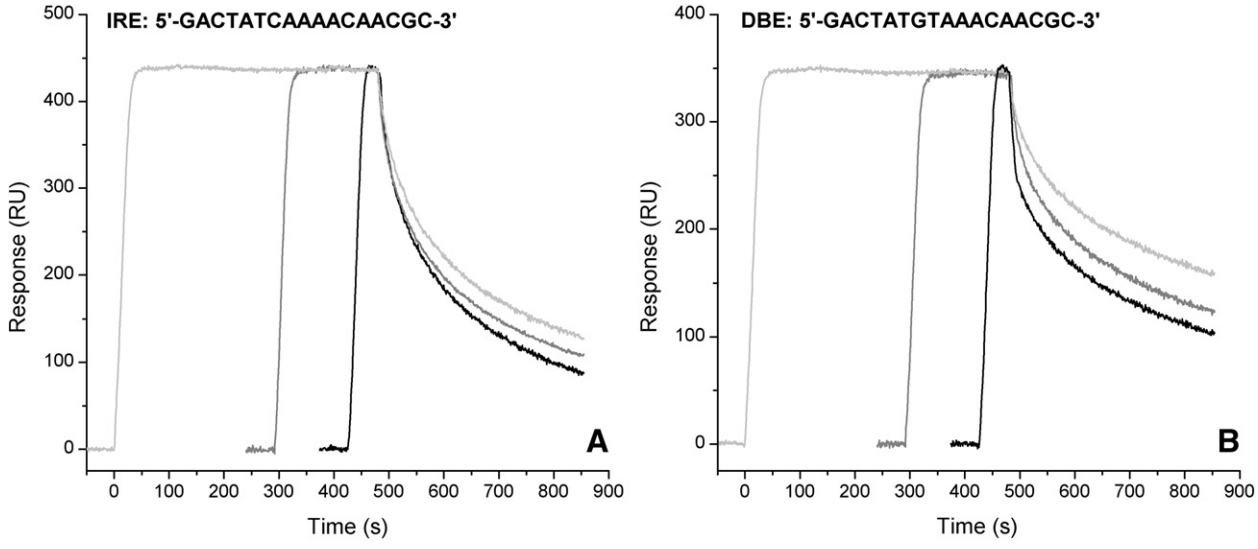

Fig. 3. Effect of different sample injection times on the dissociation rates of the sensograms. The wild-type FOXO4–DBD (300 nM) was injected at different contact times (association phase) over the sensor chip coated with dsDNA containing either the insulin-responsive (IRE) (A), or the Daf-16 family member-binding element (DBE) (B) at flow rate of 50 μl/min. The sensograms were aligned to the end of the association phases in order to highlight the differences in the dissociation rates. No normalization of the sensograms was applied.

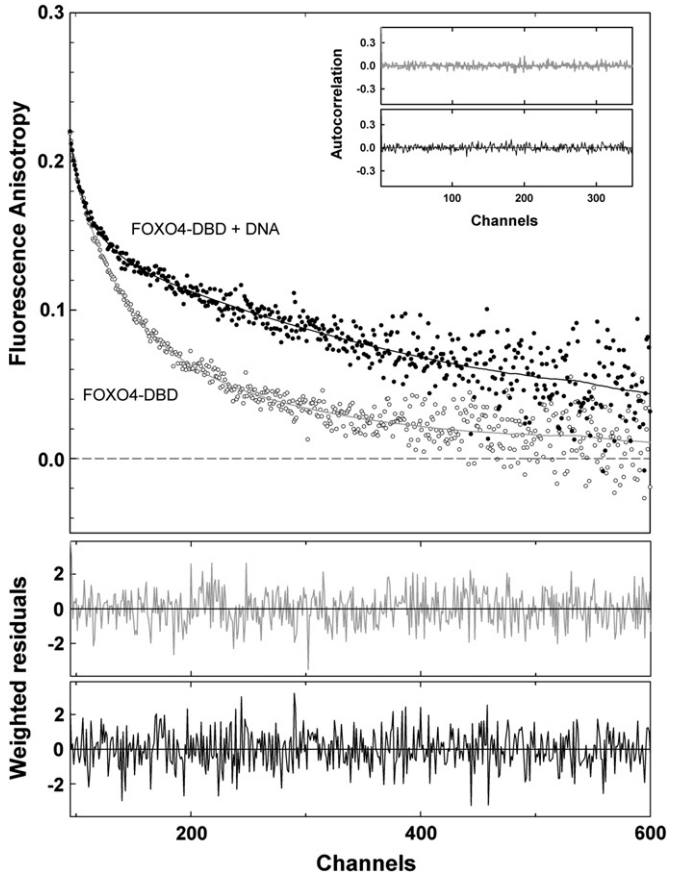

Fig. 4. Tryptophan fluorescence anisotropy decays constructed from the raw polarized decay data for FOXO4–DBD in the absence (○) and the presence (•) of dsDNA. The weighted residuals of both fits (gray, FOXO4–DBD alone; black, FOXO4–DBD + DNA) are shown in the lower panels. The quality of fits is also demonstrated by the autocorrelation functions shown in the inset (gray, FOXO4–DBD alone; black, FOXO4–DBD + DNA).

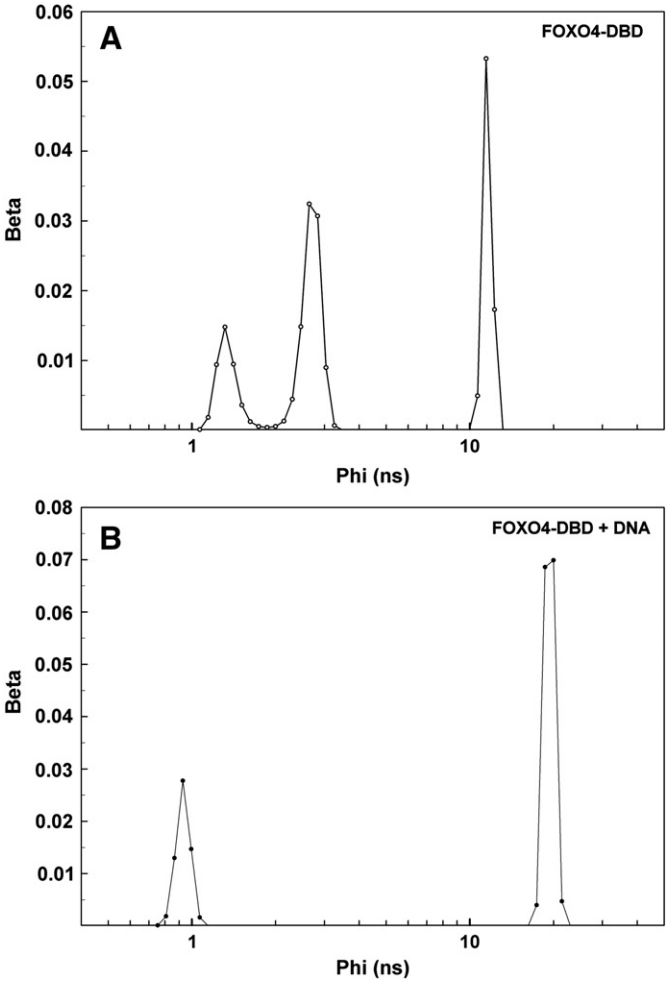

Fig. 5. Distributions of rotational correlation times of FOXO4–DBD in the absence (A) and the presence (B) of dsDNA.

differences in several regions including the N-terminal region, the loop between helices H2 and H3, and both wings W1 and W2 (Fig. 6) [10,12–14]. The largest conformational change takes place within the H2–H3 loop which adopts helical structure in the absence of DNA while in its presence is mostly unstructured. In addition, in all FOXO–DBD–DNA complexes the DNA molecule is bent toward FOXO–DBD with the major groove being slightly wider in the core-motif region [10–12].

3.4. Alanine scanning mutagenesis of amino acid residues engaged in contacts with the DNA

Based on the contact residues identified in the FOXO4–DBD–DNA complex, alanine scanning mutagenesis of FOXO4–DBD was performed followed by SPR analysis to assess the contribution of individual polar contacts for the stability of FOXO4–DBD–DNA complex as well as the kinetics of interaction. The calculated association and dissociation rate constants (k_{a1}, k_{a2}, k_{d1}, and k_{d2} from Eq. (2)) as well as K_D for interactions between prepared FOXO4–DBD variants and dsDNA containing IRE and DBE motifs are listed in Tables 3 and 4, respectively. Residuals plots for fits of the conformational change binding model to the SPR data of all FOXO4–DBD variants binding to IRE and DBE elements are shown in Figs. S5 and S6, respectively. The data analysis revealed that FOXO4–DBD WT binds both dsDNAs with K_D in the nanomolar range with the binding affinity being approximately four times higher for DBE compared to IRE (K_D of 16 ± 3 nM and 60 ± 10 nM for DBE and IRE, respectively), in a good agreement with previously published data [8,11].

Overall comparison of K_D values revealed significant decrease in the binding affinity (increase in K_D) for several mutants from various regions of DBD. In the case of binding to the IRE element, the largest decrease in the binding affinity was observed for mutants Y102F, N148A and ΔC, whereas in the case of binding to the DBE element the greatest affinity decrease were seen for mutants S101A, Y102F, N148A, H152A, K162A and ΔC. The predominant mechanism that contributed to the decreased binding affinity of these mutants is the faster dissociation rate of the encounter complex (described by the dissociation rate constant k_{d1} from Eq. (2)) compared to the wild-type. On the other hand, for mutants S142A and K162A in binding to the IRE element, and for mutants S142A and S171A in binding to the DBE element we observed an opposite effect, a significant increase in their binding affinity. It seems that the predominant mechanism that contributes to the increased binding affinity of these cases was the slower reverse rate of the conformational change (described by the dissociation rate constant k_{d2} from Eq. (2)).

3.4.1. N-terminal segment of FOXO4–DBD

Five residues from the N-terminal part of FOXO4–DBD (up to the helix H3) form either direct or water-mediated hydrogen bonds with the DNA: R95, N95, S101, Y102, and S142 (Table 1 and Fig. 1). The most significant decrease in the DNA binding affinity for IRE element was observed for mutant Y102F (Table 3), whereas in the case of DBE element for mutants S101A and Y102F (Table 4). The replacement of Y102 for Phe, which removes one hydrogen bond (non-specific contact

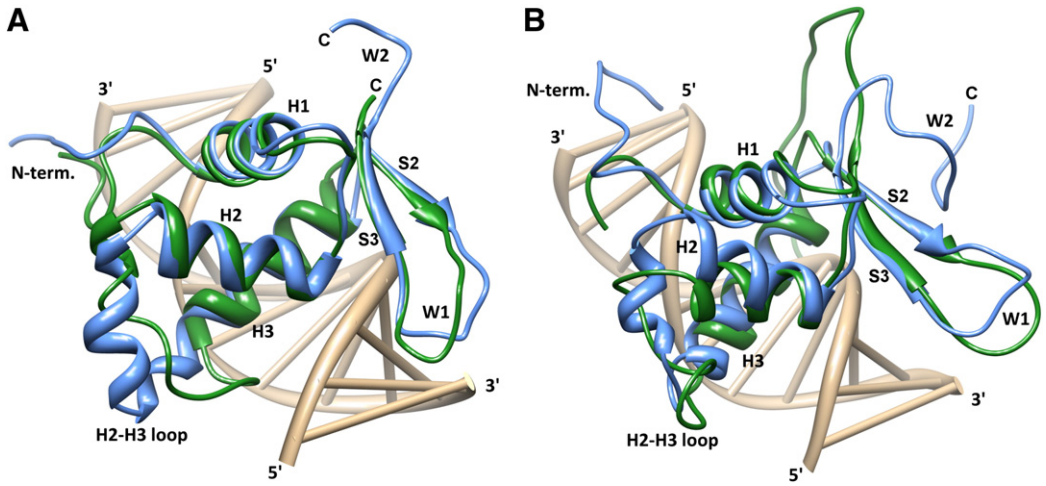

Fig. 6. Conformational changes of FOXO–DBD induced by binding to the DNA. (A) Superimposition of the FOXO4–DBD–DNA structure (shown in green [12]) with the solution structure of apo FOXO4–DBD (shown in blue [13]). (B) The superimposition of FOXO3–DBD–DNA (shown in green [10]) with the solution structure of apo FOXO3–DBD (shown in blue [14]). Secondary-structure elements are labeled according to the nomenclature typical for the winged–helix motif.

to the phosphate group of the DNA backbone) by eliminating the phenolic hydroxyl group of Y102, resulted in one of the most profound increases in the dissociation rate constant for the encounter complex formation (k_{d1}), and consequently also in K_D, among all studied mutants. This suggested the critical importance of this contact for the overall stability of the complex between FOXO4–DBD and the DNA.

3.4.2. DNA-recognition helix H3

All direct base-specific contacts between FOXO4–DBD and the core motif are made by residues N148 and H152 (Fig. 1) and their replacement significantly reduced the FOXO4–DBD binding to both IRE and DBE, with the relative decrease in the binding affinity (increase in K_D) for DBE being much higher than for IRE. Differences in the relative change in affinity for DBE and IRE were also observed upon the replacement of residue S155, which makes non-specific contact with the phosphate group of the DNA backbone. On the other hand, either no or relatively small change in K_D for both elements was observed upon the replacement of other contact residues from the helix H3: S149, R151, and N153. All these three residues are involved in water-mediated contacts, either base-specific (R151) or non-specific with phosphate groups of the DNA backbone (S149 and N153), suggesting that these interactions are not an important factor for the binding specificity nor the stability of the FOXO4–DBD–DNA complexes.

3.4.3. Flexible loops W1 and W2

Structural studies revealed that four residues from the wing W1 make either direct or water-mediated non-specific contacts with phosphate groups of the DNA backbone: K162, S171, S172 and W174 (Fig. 1). The K162A mutant exhibited somewhat decreased K_D for IRE element (change in K_D from 60 to 30 nM) but, on the other hand, significantly increased K_D for DBE element (change in K_D from 16 to 70 nM). The kinetic analysis revealed that in the case of binding to the IRE element this mutation decreased the reverse rate constant for the conformational change (k_{d2}), while in the case of binding to the DBE element it increased the dissociation rate constant for the encounter complex formation (k_{d1}). The diverse effect on binding to IRE versus DBE was

Table 3
Kinetic and binding affinity constants for the interactions between FOXO4–DBD and DNA containing IRE element.

Protein	$k_{a1} \times 10^{-5}$ (M^{-1} s^{-1})[a]	$k_{d1} \times 10^{2}$ (s^{-1})[a]	$k_{a2} \times 10^{3}$ (s^{-1})[a]	$k_{d2} \times 10^{3}$ (s^{-1})[a]	K_D (nM)[b]	Δ[cd]
WT (82–207)	1.67 ± 0.18	2.42 ± 0.31	3.65 ± 0.33	2.63 ± 0.28	60 ± 10	
R94A	1.85 ± 0.19	4.88 ± 0.56	3.74 ± 0.41	3.17 ± 0.35	120 ± 30	+
N95A	1.14 ± 0.09	3.56 ± 0.52	3.31 ± 0.34	2.35 ± 0.27	130 ± 30	+
S101A	0.87 ± 0.12	2.63 ± 0.31	3.47 ± 0.41	2.12 ± 0.25	120 ± 30	+
Y102F	1.59 ± 0.18	7.72 ± 0.83	2.99 ± 0.3	2.46 ± 0.28	220 ± 50	++
S142A	2.09 ± 0.23	1.96 ± 0.21	3.89 ± 0.46	1.68 ± 0.21	28 ± 7	*
N148A	1.84 ± 0.14	6.52 ± 0.52	2.7 ± 0.32	3.26 ± 0.35	190 ± 40	++
S149A	1.7 ± 0.21	4.62 ± 0.64	2.65 ± 0.28	1.85 ± 0.21	110 ± 30	–
R151A	0.98 ± 0.09	2.63 ± 0.38	4.8 ± 0.53	1.89 ± 0.21	80 ± 20	–
H152A	1.38 ± 0.14	4.19 ± 0.53	3.11 ± 0.37	2.25 ± 0.24	130 ± 30	+
N153A	1.25 ± 0.92	5.19 ± 0.58	3.61 ± 0.38	1.24 ± 0.14	110 ± 80	–
S155A	1.4 ± 0.17	5.13 ± 0.67	3.6 ± 0.35	1.36 ± 0.15	100 ± 20	–
K162A	1.31 ± 0.15	3.41 ± 0.37	2.92 ± 0.31	0.38 ± 0.04	30 ± 7	*
S171A	0.93 ± 0.12	2.02 ± 0.27	3.04 ± 0.33	0.84 ± 0.09	50 ± 10	–
S172A	1.6 ± 0.13	3.79 ± 0.65	3.08 ± 0.33	2.01 ± 0.22	90 ± 20	–
ΔC (82–183)	2.52 ± 0.35	28.3 ± 4.1	3.9 ± 0.43	3.18 ± 0.37	500 ± 100	+++

[a] Results are means ± S.D. from the analysis of two independent measurements carried out in duplicate.
[b] The equilibrium dissociation constant, K_D, was determined as $1/[(k_{a1}/k_{d1}) \times (1 + k_{a2}/k_{d2})]$ assuming conformational change model. Error was calculated from the errors in determination of rate constants.
[c] Relative increase in K_D with respect to WT: (−), <2×; (+), 2–3×; (++), 3–4×; (+++), >4×.
[d] (*) denotes a significant decrease in K_D with respect to WT.

Table 4
Kinetic and binding affinity constants for the interactions between FOXO4–DBD and DNA containing DBE element.

Protein	$k_{a1} \times 10^{-5}$ (M^{-1} s^{-1})[a]	$k_{d1} \times 10^{2}$ (s^{-1})[a]	$k_{a2} \times 10^{3}$ (s^{-1})[a]	$k_{d2} \times 10^{3}$ (s^{-1})[a]	K_D (nM)[b]	Δ[cd]
WT (82–207)	2.02 ± 0.19	1 ± 0.13	2.65 ± 0.24	1.32 ± 0.09	16 ± 3	
R94A	2.61 ± 0.35	1.93 ± 0.26	3.65 ± 0.4	2.33 ± 0.26	29 ± 7	–
N95A	1.37 ± 0.14	2.27 ± 0.25	3.47 ± 0.36	1.55 ± 0.18	50 ± 10	++
S101A	0.97 ± 0.11	2.04 ± 0.26	2.82 ± 0.31	1.42 ± 0.17	70 ± 20	+++
Y102F	2.14 ± 0.27	4.49 ± 0.58	3.49 ± 0.38	1.97 ± 0.21	80 ± 20	+++
S142A	2.6 ± 0.31	0.77 ± 0.09	2.68 ± 0.25	0.84 ± 0.1	7 ± 2	*
N148A	2.14 ± 0.23	4.59 ± 0.49	2.2 ± 0.24	3.79 ± 0.45	140 ± 30	+++
S149A	2.61 ± 0.35	2.06 ± 0.19	2.26 ± 0.27	0.77 ± 0.09	20 ± 5	–
R151A	1.11 ± 0.18	1.25 ± 0.1	3.61 ± 0.38	1.29 ± 0.16	30 ± 7	–
H152A	1.47 ± 0.19	3.6 ± 0.42	3.66 ± 0.39	1.61 ± 0.2	80 ± 20	+++
N153A	2.43 ± 0.29	3.36 ± 0.38	2.75 ± 0.31	0.97 ± 0.12	36 ± 8	+
S155A	1.44 ± 0.19	3.56 ± 0.48	4.79 ± 0.52	1.56 ± 0.17	60 ± 20	++
K162A	1.45 ± 0.17	2.55 ± 0.36	2.64 ± 0.29	1.53 ± 0.16	70 ± 20	+++
S171A	1.55 ± 0.19	1.07 ± 0.09	2.34 ± 0.25	0.14 ± 0.02	4 ± 1	*
S172A	2.04 ± 0.22	1.63 ± 0.18	3.14 ± 0.34	1.43 ± 0.15	25 ± 5	–
ΔC (82–183)	1.9 ± 0.28	25.2 ± 3.9	4.8 ± 0.52	3.41 ± 0.41	600 ± 100	+++

[a] Results are means ± S.D. from the analysis of two independent measurements carried out in duplicate.
[b] The equilibrium dissociation constant, K_D, was determined as $1/[(k_{a1}/k_{d1}) \times (1 + k_{a2}/k_{d2})]$ assuming conformational change model. Error was calculated from the errors in determination of rate constants.
[c] Relative increase in K_D with respect to WT: (−), <2×; (+), 2–3×; (++), 3–4×; (+++), >4×.
[d] (*) denotes a significant decrease in K_D with respect to WT.

also observed for the S171A mutant that showed no change in binding affinity for the IRE element but significantly decreased K_D for the DBE element through the reduction of the rate constant k_{d2}. Mutation S172A had no effect on FOXO4–DBD binding to both tested elements. We were unable to test the role of W174 as its substitution to Phe caused aggregation of prepared FOXO4–DBD protein.

To assess the role of flexible wing W2 in the stability of the FOXO4–DBD–DNA complex we used the C-terminally truncated FOXO4–DBD (amino acids 82–183). The results from SPR measurements showed that the removal of wing W2 dramatically reduced the DNA-binding affinity of FOXO4–DBD for both IRE and DBE elements (Tables 3 and 4). In both cases the C-terminally truncated protein exhibited much faster dissociation rate of the encounter complex (described by the dissociation rate constant k_{d1}) compared to the wild-type, thus confirming that the wing W2 region, although being very flexible, is very important for the stability of FOXO–DBD–DNA complexes, and especially for the formation of the encounter protein–DNA complexes.

4. Discussion

FOXO proteins recognize both motifs through similar patterns of direct and water-mediated side chain-base contacts and numerous non-specific contacts to the DNA backbone. Brent et al. [11] by comparing crystal structures of FOXO1–DBD bound to IRE and DBE suggested that difference in the binding affinity for these two motifs results from different hydrogen-bonding patterns around side chains of N211 and H215 (N148 and H152 in FOXO4). Structural studies also revealed that non-specific contacts to the phosphate groups of the DNA backbone, mainly those contributed by flexible wing W2, are an important factor in the modulation of FOXO–DNA interactions. Since even small differences in DNA-binding affinity for different response elements might potentially influence gene regulations by these motifs (e.g. the timing of gene expression [5]), the detailed understanding of bases of protein–DNA recognition is of utmost importance. In this work, we studied the real-time kinetics of the interaction between FOXO4–DBD and the DNA as well as the role of polar contacts observed at the FOXO4–DBD–DNA interface (Table 1 and Fig. 1) for binding affinity and specificity using SPR analysis.

The comparison of apo- and DNA-bound structures indicates that both FOXO–DBD and the DNA undergo a structural transition during the complex formation [10–14]. The present real-time kinetics study shows that the interaction between FOXO4–DBD and the dsDNA containing either the DBE or the IRE element is preferably described by using a conformational change binding kinetics that includes a structural change of FOXO4–DBD upon the binding to the DNA. Next, the time-resolved tryptophan fluorescence anisotropy decay measurements were used to provide a direct experimental evidence of suggested conformational change of FOXO4–DBD upon its binding to the DNA. These experiments showed a significant restriction of segmental motions of tryptophan residues upon the complex formation, thus confirming that FOXO4–DBD undergoes a structural change connected with significant loss of flexibility (Table 2 and Figs. 4 and 5). Our data, therefore, strongly suggest that the structural transition is an inherent part of the interaction between FOXO–DBD and the DNA.

Next, we performed alanine scanning mutagenesis of FOXO4–DBD amino acid residues engaged in polar contacts with the DNA to assess their contribution for both the binding affinity and the specificity. The SPR analysis revealed that the majority, but not all, of studied residues play an important role in the overall stability of FOXO4–DBD–DNA complexes. However, the contributions of individual contact residues, including those contributing non-specific contacts to the phosphate groups of the DNA backbone, significantly differ between two studied DNA motifs (Tables 3 and 4) suggesting that these non-specific contacts play a role in binding specificity of FOXO–DBD. The majority of generated FOXO4–DBD variants exhibits the faster dissociation rate of the encounter complex (described by the dissociation rate constant k_{d1} from Eq. (2)) compared to FOXO4–DBD WT. The most significant reduction in binding affinity was observed for the deletion mutant ΔC with the missing wing W2, mutants of residues involved in base-specific contacts (N148 and H152), and, interestingly, mutant of Y102 which is involved in non-specific contact with the phosphate group of the DNA backbone. Structural studies showed that residue Y102 is a part of a cluster of hydrophobic residues consisting of W97 from the N-terminal loop, Y102 from the helix H1, Y133 and F134 from the loop between helices H2 and H3, and W146 from the N-terminal part of helix H3 (Fig. 1). It has previously been shown that residues from these regions affect the DNA-binding properties of various FOX transcription factors, presumably through the repositioning of the recognition helix H3 [18,19,28,29]. Thus, we may speculate that the removal of hydrogen bond between Y102 and the DNA backbone affects the presentation of the helix H3 to the major groove of the DNA, thus significantly reducing the binding affinity for both tested motifs. In addition, our SPR data show that mutations within the N-terminal

segment (N95A, S101A and Y102F) have more distinct effect on interaction with DBE rather than IRE (Tables 3 and 4). These residues make non-specific contacts with the phosphate groups of the DNA backbone at the border of the core motif where sequences of IRE and DBE elements differ. This suggests that the N-terminal segment might play a role in DNA-binding specificity of FOXO proteins.

Compared with other FOX proteins, all members of FOXO subfamily contain between helices H2 and H3 a five-amino-acid insertion (sequence KGDSN) of unknown function. Structural studies revealed either no (for FOXO1–DBD and FOXO3–DBD) or very few (for FOXO4–DBD) contacts of this region with the DNA [10–12]. Fig. 1 shows the interaction observed in the FOXO4–DBD–DNA complex where one of these residues (S142) makes several non-specific contacts with the phosphate groups of the DNA. As can be noticed from Tables 3 and 4, the S142A mutation did affect (significantly increases) the binding affinity suggesting that this region plays some modulatory role in FOXO binding to the DNA.

Highly conserved residues from helix H3 make extensive contacts with bases of the core sequence via both direct and water-mediated hydrogen bonds as well as van der Waals contacts [10–12]. Since all direct base-specific contacts are made by residues N148 and H152 (Fig. 1) it is not surprising that replacement of both these residues significantly reduced the FOXO4–DBD binding to both IRE and DBE, with the effect being much higher for DBE than for IRE (Tables 3 and 4). It is likely that these differences reflect different pattern of hydrogen-bonding interactions between side-chains of these residues and the core sequences of DBE and IRE elements [11].

It has previously been suggested that the flexible loop W1 located between strands S2 and S3 (Fig. 1), which differs both in length and its amino acid composition among different FOX proteins, plays various roles in the mediation of DNA recognition and the stability of FOX–DBD–DNA complexes [10]. Observed differences in the binding kinetics of K162A and S171A mutants for IRE vs DBE cannot be explained by different patterns of contacts. Crystal structures of FOXO1–DBD–DNA complexes show exactly the same interactions between this region and the backbone of both IRE and DBE elements [11]. Therefore, it seems that observed differences rather reflect distinct physico-chemical properties of studied DNA elements resulting from sequence variation.

It is well established that the highly flexible loop wing W2 located at the C-terminus of FOXO–DBD plays an important, although not fully understood, role in FOXO binding to the DNA. This region contains several sites of post-translational modifications whose modification or mutagenesis have been shown to cause a moderate reduction in the FOXO DNA-binding affinity [10,11,15,16]. In the structure of FOXO3–DBD–DNA complex, the wing W2 adopts a coiled structure and its basic residues make ionic contacts with the phosphate groups in the major groove without any base-specific contacts [10]. However, high values of B-factors reported for its residues suggest high flexibility of this region. In all three reported FOXO1–DBD–DNA structures the wing W2 is completely disordered and, thus, its interaction with DNA is unclear [11]. Its removal, however, severely reduced the FOXO1–DBD binding to the DNA. Our data show that the removal of this segment dramatically increases the dissociation rate of the encounter complex (rate constant k_{d1} from Eq. (2)) for both IRE and DBE. In the case of binding to DBE, the C-terminally truncated FOXO4–DBD ΔC exhibits also changed kinetics of the structural transition between the encounter complex and the final docked structure (described by rate constants k_{a2} and k_{d2}). Thus, this region might also be involved in fine-tuning of DNA-binding specificity of FOXO proteins.

Taken together, our data show that when binding to the DNA, FOXO4–DBD undergoes a structural change connected with the significant loss of flexibility. The interaction between FOXO4–DBD and DNA is preferably described by using a conformational change binding model and not only the base-specific but also non-specific polar contacts to the phosphate groups of the DNA backbone from various regions of DBD are an important factor contributing to both the DNA-binding affinity and specificity of FOXO proteins.

Acknowledgments

This work was supported by the Ministry of Education, Youth, and Sports of the Czech Republic (Research Project MSM0021620857); Czech Science Foundation (Projects P305/11/0708 and P207/11/0717); and Academy of Sciences of the Czech Republic (Research Projects RVO: 67985823 and RVO: 61388971). We wish to thank P. Novotna from the Department of Physics and Measurements, Institute of Chemical Technology, Prague for measuring the CD spectra.

Appendix A. Supplementary data

Supplementary data to this article can be found online at http://dx.doi.org/10.1016/j.bpc.2013.09.002.

References

[1] D.R. Calnan, A. Brunet, The FoxO code, Oncogene 27 (2008) 2276–2288.
[2] D. Weigel, H. Jackle, The fork head domain—a novel DNA-binding motif of eukaryotic transcription factors, Cell 63 (1990) 455–456.
[3] K.L. Clark, E.D. Halay, E. Lai, S.K. Burley, Co-crystal structure of the HNF-3/fork head DNA-recognition motif resembles histone H5, Nature 364 (1993) 412–420.
[4] A.B. Georges, B.A. Benayoun, S. Caburet, R.A. Veitia, Generic binding sites, generic DNA-binding domains: where does specific promoter recognition come from? FASEB J. 24 (2010) 346–356.
[5] J. Gaudet, S.E. Mango, Regulation of organogenesis by the *Caenorhabditis elegans* FoxA protein PHA-4, Science 295 (2002) 821–825.
[6] W.H. Biggs 3rd, J. Meisenhelder, T. Hunter, W.K. Cavenee, K.C. Arden, Protein kinase B/Akt-mediated phosphorylation promotes nuclear exclusion of the winged helix transcription factor FKHR1, Proc. Natl. Acad. Sci. U. S. A. 96 (1999) 7421–7426.
[7] S. Guo, G. Rena, S. Cichy, X. He, P. Cohen, T. Unterman, Phosphorylation of serine 256 by protein kinase B disrupts transactivation by FKHR and mediates effects of insulin on insulin-like growth factor-binding protein-1 promoter activity through a conserved insulin response sequence, J. Biol. Chem. 274 (1999) 17184–17192.
[8] T. Furuyama, T. Nakazawa, I. Nakano, N. Mori, Identification of the differential distribution patterns of mRNAs and consensus binding sequences for mouse DAF-16 homologues, Biochem. J. 349 (2000) 629–634.
[9] W.H. Biggs 3rd, W.K. Cavenee, K.C. Arden, Identification and characterization of members of the FKHR (FOXO) subclass of winged-helix transcription factors in the mouse, Mamm. Genome 12 (2001) 416–425.
[10] K.L. Tsai, Y.J. Sun, C.Y. Huang, J.Y. Yang, M.C. Hung, C.D. Hsiao, Crystal structure of the human FOXO3a-DBD/DNA complex suggests the effects of post-translational modification, Nucleic Acids Res. 35 (2007) 6984–6994.
[11] M.M. Brent, R. Anand, R. Marmorstein, Structural basis for DNA recognition by FOXO1 and its regulation by posttranslational modification, Structure 16 (2008) 1407–1416.
[12] E. Boura, L. Rezabkova, J. Brynda, V. Obsilova, T. Obsil, Structure of the human FOXO4–DBD–DNA complex at 1.9 A resolution reveals new details of FOXO binding to the DNA, Acta Crystallogr. D: Biol. Crystallogr. 66 (2010) 1351–1357.
[13] J. Weigelt, I. Climent, K. Dahlman-Wright, M. Wikstrom, Solution structure of the DNA binding domain of the human forkhead transcription factor AFX (FOXO4), Biochemistry 40 (2001) 5861–5869.
[14] F. Wang, C.B. Marshall, K. Yamamoto, G.Y. Li, M.J. Plevin, H. You, T.W. Mak, M. Ikura, Biochemical and structural characterization of an intramolecular interaction in FOXO3a and its binding with p53, J. Mol. Biol. 384 (2008) 590–603.
[15] E. Boura, J. Silhan, P. Herman, J. Vecer, M. Sulc, J. Teisinger, V. Obsilova, T. Obsil, Both the N-terminal loop and Wing W2 of the forkhead domain of transcription factor foxo4 are important for DNA binding, J. Biol. Chem. 282 (2007) 8265–8275.
[16] H. Matsuzaki, H. Daitoku, M. Hatta, H. Aoyama, K. Yoshimochi, A. Fukamizu, Acetylation of FOXO1 alters its DNA-binding ability and sensitivity to phosphorylation, Proc. Natl. Acad. Sci. U. S. A. 102 (2005) 11278–11283.
[17] J. Silhan, P. Vacha, P. Strnadova, J. Vecer, P. Herman, M. Sulc, J. Teisinger, V. Obsilova, T. Obsil, 14-3-3 protein masks the DNA binding interface of forkhead transcription factor FOXO4, J. Biol. Chem. 284 (2009) 19349–19360.
[18] S. Pierrou, M. Hellqvist, L. Samuelsson, S. Enerback, P. Carlsson, Cloning and characterization of seven human forkhead proteins: binding site specificity and DNA bending, EMBO J. 13 (1994) 5002–5012.
[19] D.G. Overdier, A. Porcella, R.H. Costa, The DNA-binding specificity of the hepatocyte nuclear factor 3/forkhead domain is influenced by amino-acid residues adjacent to the recognition helix, Mol. Cell. Biol. 14 (1994) 2755–2766.
[20] T. Shiyanova, X. Liao, The dissociation rate of a winged helix protein-DNA complex is influenced by non-DNA contact residues, Arch. Biochem. Biophys. 362 (1999) 356–362.
[21] M.J. van Dongen, A. Cederberg, P. Carlsson, S. Enerback, M. Wikstrom, Solution structure and dynamics of the DNA-binding domain of the adipocyte-transcription factor FREAC-11, J. Mol. Biol. 296 (2000) 351–359.

[22] G. Krauss, D. Riesner, G. Maass, Mechanism of discrimination between cognate and non-cognate tRNAs by phenylalanyl-tRNA synthetase from yeast, Eur. J. Biochem. 68 (1976) 81–93.
[23] D. Riesner, A. Pingoud, D. Boehme, F. Peters, G. Maass, Distinct steps in the specific binding of tRNA to aminoacyl-tRNA synthetase. Temperature-jump studies on the serine-specific system from yeast and the tyrosine-specific system from *Escherichia coli*, Eur. J. Biochem. 68 (1976) 71–80.
[24] C.A. Lipschultz, Y. Li, S. Smith-Gill, Experimental design for analysis of complex kinetics using surface plasmon resonance, Methods 20 (2000) 310–318.
[25] L. Rezabkova, M. Kacirova, M. Sulc, P. Herman, J. Vecer, M. Stepanek, V. Obsilova, T. Obsil, Structural modulation of phosducin by phosphorylation and 14-3-3 protein binding, Biophys. J. 103 (2012) 1960–1969.
[26] J. Vecer, P. Herman, Maximum entropy analysis of analytically simulated complex fluorescence decays, J. Fluoresc. 21 (2011) 873–881.
[27] D. Veisova, L. Rezabkova, M. Stepanek, P. Novotna, P. Herman, J. Vecer, T. Obsil, V. Obsilova, The C-terminal segment of yeast BMH proteins exhibits different structure compared to other 14-3-3 protein isoforms, Biochemistry 49 (2010) 3853–3861.
[28] I. Marsden, Y. Chen, C. Jin, X. Liao, Evidence that the DNA binding specificity of winged helix proteins is mediated by a structural change in the amino acid sequence adjacent to the principal DNA binding helix, Biochemistry 36 (1997) 13248–13255.
[29] I. Marsden, C. Jin, X. Liao, Structural changes in the region directly adjacent to the DNA-binding helix highlight a possible mechanism to explain the observed changes in the sequence-specific binding of winged helix proteins, J. Mol. Biol. 278 (1998) 293–299.